Radiative Double-Electron Capture by Bare and One-Electron Ions on Gas Targets

D. S. La Mantia, P. N. S. Kumara, S. L. Buglione, C. P. McCoy, C. J. Taylor, J. S. White, A. Kayani, and J. A. Tanis

Radiative Double Electron Capture by Bare and One-Electron Ions on Gas Targets

D. S. La Mantia,[*] P. N. S. Kumara, S. L. Buglione, C. P. McCoy, C. J. Taylor, J. S. White, A. Kayani, and J. A. Tanis

Western Michigan University, Kalamazoo, MI 49008 U.S.A.

(Dated: March 4, 2020)

Radiative double electron capture (RDEC) involves the transfer of two electrons with the simultaneous emission of a single photon. This process, which can be viewed as the inverse of double photoionization, has been studied for 2.11 MeV/u F^{9+} and F^{8+} ions striking gas targets of N_2 and Ne. The existence of RDEC is conclusively shown for both targets and the results are compared with earlier O^{8+} and F^{9+} findings for thin-foil carbon and with theory. The data for the carbon target showed some evidence for the existence of RDEC but the interpretation was clouded by high-probability, unavoidable multiple collisions causing the exiting charge state to be increased.

In the collision between an ion and an atom the possibility of the capture of two electrons simultaneous with the emission of a single photon was suggested by Miraglia and Gravielle [1]. This process is referred to as radiative double electron-capture (RDEC) and for ion-atom collisions can be considered the inverse of double photoionization. The study of RDEC where two electrons are involved promises new insight into electron correlation and the role it plays in quantum electrodynamics. The ability to gain information on correlation without the effects of neighboring electrons is important to fundamental studies of RDEC and double photoionization and to applications in astrophysics and in plasma physics.

Previously, RDEC was reported for fully-stripped oxygen and fluorine ions striking thin-foil carbon targets [2, 3]. Multiple collisions in the foil targets caused the outgoing charge state to increase, clouding interpretation of the data and leaving questions regarding the existence and magnitude of RDEC. The present work investigates RDEC for gas targets under single-collision conditions and compares the results with those for solid targets.

RDEC is related to radiative electron capture, where a single electron is captured to a bound state with the simultaneous emission of a photon [4, 5], and is considered the ion-atom analog of radiative recombination. The energy schematics for REC and RDEC are shown in Fig. 1, with the photon energies given by:

$$E_{REC} = K_t + B_p - B_t + (\vec{v} \cdot \vec{p}) \tag{1}$$

$$E_{RDEC} = 2K_t + B_p^1 + B_p^2 - B_t^1 - B_t^2 + (\vec{v} \cdot \vec{p})^1 + (\vec{v} \cdot \vec{p})^2 \tag{2}$$

Here, K_t is the kinetic energy of the target electrons as seen from the projectile rest frame, B_p are positive projectile binding energies, B_t are positive target binding energies, $\vec{v}$ is the projectile velocity, and $\vec{p}$ is the momentum of the bound target electron, with the superscripts 1 and 2 referring to the captured electrons. The $\vec{v} \cdot \vec{p}$ term represents the contribution of the Compton profile [6] of the captured electrons along the beam direction, resulting in broadening of the transition peak.

Several attempts were made to observe RDEC [7–9] without definitive results using mid- to high-Z, high-energy projectiles on thin-foil and gaseous targets. Early
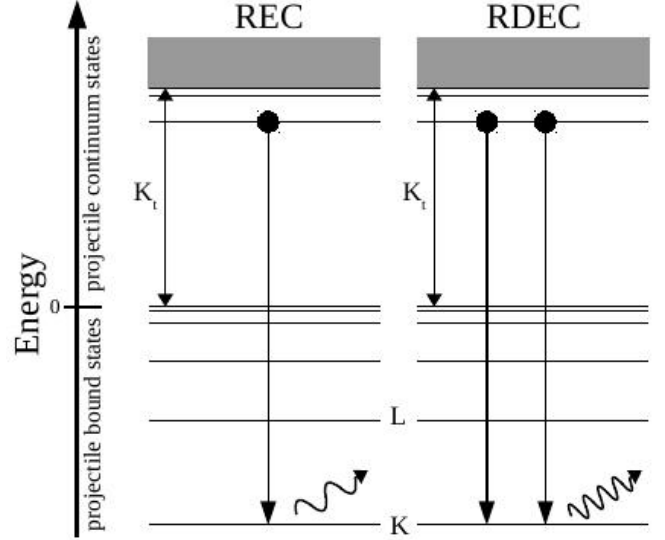

FIG. 1. Energy schematic for the radiative capture of one (REC) or two (RDEC) electrons from a target bound state. K_t is the kinetic energy of the captured electron(s) as seen from the projectile reference frame. The captured electrons can go to any available projectile shell.

theoretical studies [10, 11] and more recent investigations [12, 13] suggested mid-Z, lower-energy projectiles would yield better results with larger cross sections. The first successful experimental observation of RDEC was done for 2.38 MeV/u O^{8+} projectiles [2] incident on thin-foil carbon, followed by 2.11 MeV/u F^{9+} also on carbon [3], which however suffered from contaminants in the target. Multiple-collision effects were present as expected for thin-foil carbon, causing the RDEC events to be spread over single and double capture outgoing channels.

In this Letter definitive evidence for RDEC by fully-stripped, and also one-electron, fluorine ions colliding with N_2 and Ne are reported. Use of gas targets eliminated the possibility of multiple-collision effects. One-electron ions are expected to have reduced probability for RDEC because of the electron already present in the K shell. Cross sections are determined and compared with theoretical calculations to the extent possible [12, 14].
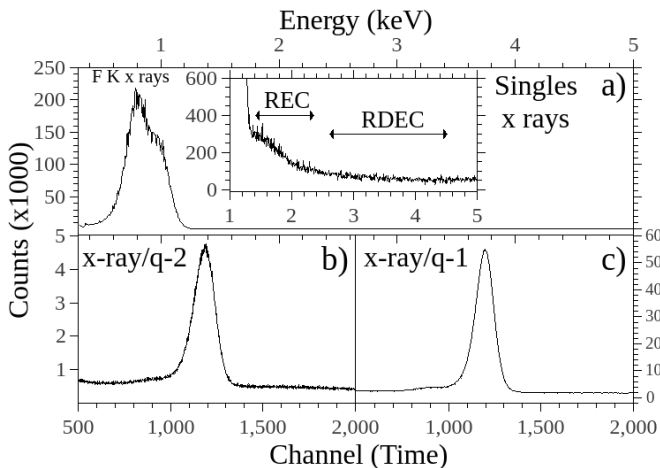
FIG. 2. Sums of collected (a) x-ray singles events, and (b) x-ray/doubly charge-changed (q-2) and (c) x-ray/singly charge-changed (q-1) coincidence events for 2.11 MeV/u F^{9+} + N_2.

This work was performed using the tandem Van de Graaff accelerator facility at Western Michigan University [15]. Fluorine ions of charge state 9+ or 8+ were obtained and collimated to a diameter $\sim$3 mm before entering the collision chamber consisting of a 3.65 cm differentially-pumped gas cell. Target gas pressures of 8 mTorr for N_2 and 15 mTorr for Ne were used giving total charge exchanges of $\sim$3-4%. A Si(Li) x-ray detector with effective area $\sim$60 mm^2 was mounted at 90$^{\mathrm{o}}$ to the beam at a distance of 17 mm. The detector had a 0.4 μm polymer window with an efficiency of nearly 85% at $\sim$1 keV (F K-x-ray energy).

After passing through the interaction region, the ion beam was analyzed into its charge-state components using a dipole magnet. The primary beam was collected in a Faraday cup, measured with a Keithley electrometer, and digitized to give the number of incident particles. Doubly (q-2) and singly (q-1) charge-changed beam components were collected with silicon surface-barrier detectors. Signals from the x-ray and particle detectors were sent to an event-mode data acquisition system from which coincidences between collected photons and particles were sorted, with x rays in certain energy ranges assigned to their respective charge-changed particles, or vice versa.

Shown in Fig. 2 are the sums of the collected (a) x ray singles events and (b) x-ray/doubly charge-changed (q-2) and (c) x-ray/singly charge-changed (q-1) particle coincidence events for 2.11 MeV/u F^{9+} + N_2. Similar spectra were obtained for the Ne target. All the spectra taken for F^{9+} and F^{8+} on N_2 and Ne were collected for $\sim$1.0x10^{12} incident particles. Helium was also tried as a target but the counting rate was much lower than for N_2 or Ne, giving only three counts attributed to RDEC. For N_2 and Ne, runs were taken with no gas to ensure that REC and RDEC did not take place in the absence of the target.

TABLE I. RDEC transition energies (in keV) for 2.11 MeV/u F^{9+} projectiles. V refers to valence (quasi-free) electrons.

RDEC Transition	N_2	Ne
KK→KL	2.79	1.87
VK→KL	3.20	2.74
KK→KK	3.53	2.61
VV→KL	3.61	3.61
VK→KK	3.94	3.48
VV→KK	4.35	4.35

Most prominent in the spectrum of Fig. 2a are the F projectile K x rays, with the REC events occurring on the high-energy side of this peak. Above the REC, appearing as background, are the RDEC events in the region indicated. The data reported for each projectile charge state and target required $\sim$500 hours of measurement.

The RDEC transition energies for 2.11 MeV F^{9+}+N_2 and Ne are shown in Table I. The notation V represents valence (quasi-free) electrons. For Ne, the REC region (not listed) extends to 2.25 keV (the V→K transition) with the RDEC region starting at 1.87 keV (KK→KL). For F^{8+} projectiles, the binding energy is about 150 eV lower and RDEC transitions to the KK shells are not possible, leaving just three possible transitions.

The x-ray/q-2 particle spectra shown in Fig. 2b were sorted on emitted x rays from the RDEC energy region indicated in Fig. 2a for F^{9+} and similarly for F^{8+} (not shown) incident on N_2 and the results are displayed in Figs. 3a,b. A significant difference is seen in the number of events for F^{9+} and F^{8+}, presumably related to the number of K-shell vacancies in the projectile (two versus one) and, therefore, the allowed RDEC transitions. The spectra were integrated with regions above and below the x-ray/q-2 peak used to obtain the background to be subtracted. This gave totals of $\sim$70 and $\sim$12 RDEC counts for F^{9+} and F^{8+}. The events in Figs. 3a,b appear at slightly larger channel numbers (longer times) than the x-ray/q-2 peak of Fig. 2b and give a sharp peak at about channel 1325.

The coincidence events in the x-ray/q-2 spectrum of Fig. 2b were sorted on the REC energy region of Fig. 2a and analyzed in the same way giving the results shown in Figs. 3c,d. REC events in the x-ray/q-2 channel occur because the probability of capturing a second, uncorrelated electron is rather large. For these spectra, the peaks come at about channel 1275, slightly below those for the RDEC peaks seen in Figs. 3a,b, due to small differences in the electronic rise times of the REC and RDEC pulses.

The events in the x-ray/q-1 spectra shown in Figs. 3e,f were obtained by sorting Fig. 2c (only shown for F^{9+}) using the REC region from Fig. 2a. Here, the peak channel position is unrelated to the REC peak position in Figs. 3c,d because different particle detectors and electronic modules were used and the delay, although close,
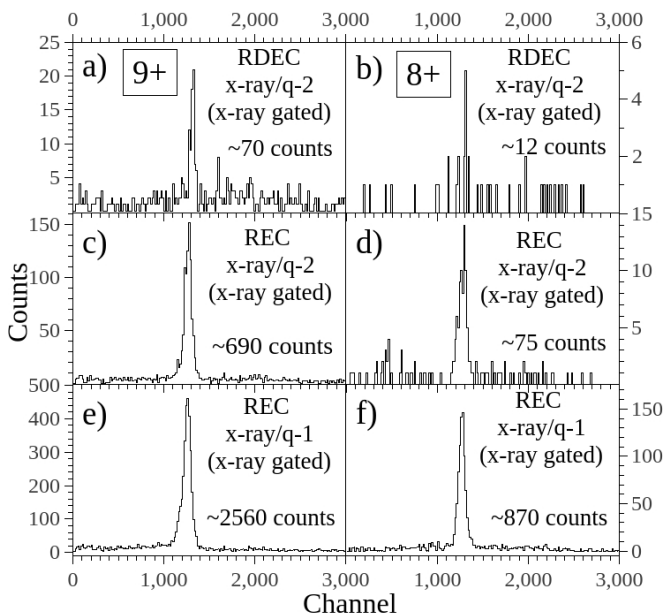
FIG. 3. Spectra for 2.11 MeV/u F^{9+} (left) and F^{8+} (right) $+N_2$: (a),(b) x-ray/q-2 events from Fig. 2b sorted on x rays from the RDEC energy range (Fig. 2a); (c),(d) x-ray/q-2 events from Fig. 2b and (e),(f) x-ray/q-1 events from Fig. 2c sorted on x rays from the REC energy range (Fig. 2a).
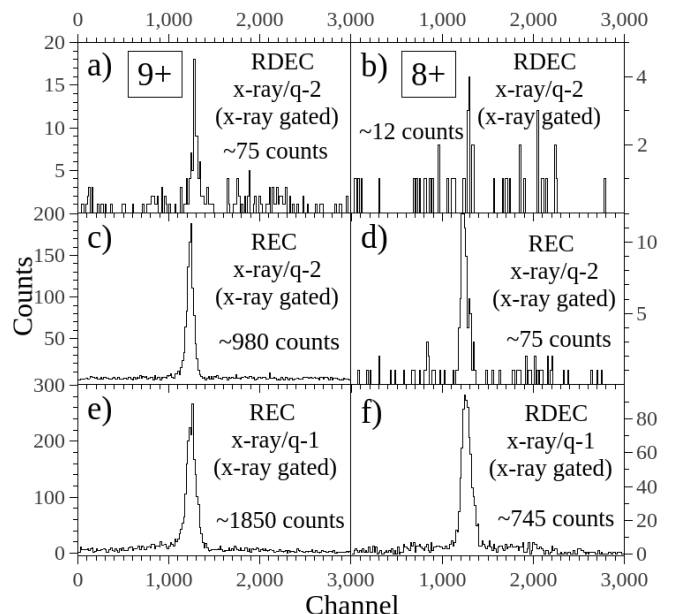

FIG. 4. Spectra for 2.11 MeV /u F^{9+} (left) and F^{8+} (right) $+Ne$: (a),(b) x-ray/q-2 events from spectra similar to Fig. 2b sorted on x rays from the RDEC energy range (spectrum like Fig. 2a); (c),(d) x-ray/q-2 events from spectra like Fig. 2b and (e),(f) x-ray/q-1 events from spectra like Fig. 2c sorted on x rays from the REC energy range (spectrum like Fig. 2a).

was not precisely the same. The events in Figs. 3c,d can then be added to those of Figs. 3e,f, respectively, to give the total K-REC events observed for F^{9+} and F^{8+}, which were 3250 and 945. These numbers do not include the L-REC transitions, which lie under the F K x rays. The x-ray/q-1 coincidence spectra (Fig. 2c) were also sorted on the RDEC region (Fig. 2a), but showed no evidence of peaks indicating that RDEC events do not occur in the spectrum one charge state higher.

The investigation was done for the same projectiles and similar numbers of collected particles incident on the Ne target. Figs. 4a,b show the x-ray/q-2 events for F^{9+} and F^{8+} projectiles for an RDEC region similar to that of Fig. 2a for N_2, with the results for Ne similar to those for N_2. The Ne RDEC peak comes at the same channel (about 1325) as for N_2, with the numbers of RDEC counts for F^{9+} and F^{8+} on Ne being ~75 and ~12. The K-REC spectra associated with x-ray/q-2 (Figs. 4c,d) and x-ray/q-1 (Figs. 4e,f) have the same features as those for the N_2 target, with the total number of K-REC counts being ~2830 and ~820 for F^{9+} and F^{8+}. Again, these numbers do not include the REC events that fall under the main F K x-ray peak.

The resulting x-ray spectrum associated with double charge exchange, i.e., x-ray/q-2 (see Figs. 2a and 2b), for 2.11 MeV/u F^{9+} incident on N_2 is shown in Fig. 5. The REC peak is readily seen between the energies of ~1.4-2.4 keV. Beyond REC lies the RDEC region. The number of RDEC x-ray events (~70) agrees with that from the

x-ray/q-2 spectra of Fig. 3a, as it should. Intensities above zero, after background subtraction, can be seen in the region 2.6-4.6 keV and are attributed to x-rays from RDEC, as predicted by the lines listed in Table I.

These predicted lines are broadened by the Compton profiles of the transitions shown by the curves in the figures (normalized to the peaks). Although Fig. 5 shows all the transitions to contribute, the combinations of the KK→KL and VK→KL transitions are the strongest, providing the most to the RDEC intensity. This result indicates a stronger correlation in these final states, in agreement with predictions of Nefiodov [13].

These results show that in the initial state there is correlation involving two K electrons, two V electrons, or one K and one V electron, although some of the combinations have stronger RDEC intensities than others. Also, there seems to be a preference in the case of incident fully-stripped projectiles for transitions involving one final K electron and one final L electron, with transitions for both electrons going to the K shell less likely. The origin of this may lie in the relative velocity of the projectile to the target, resulting in a factor that changes as the velocity changes. On the other hand, for one-electron projectiles (F^{8+}), which have one K-shell vacancy and a fully-open L shell, the overall probability of RDEC is considerably lower. Although a factor of two or four might be explained, a factor of six (see Table II) is seen in the data. This point needs further investigation.
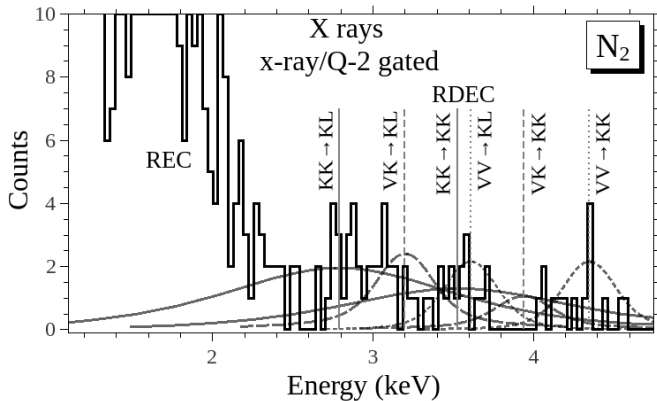
FIG. 5. X-ray spectrum obtained from events sorted on the x-ray/q-2 coincidence spectrum (Fig. 2b) for 2.11 MeV /u F^{9+} incident on N_2. The smooth curves under the RDEC region show the calculated Compton profiles of the transitions arbitrarily normalized to the data. The following scheme is used based on the initial state of the transition: VV is indicated by the short dashed lines, VK by the long dashed lines, and KK by the solid lines.

From Eqs. 1 and 2, the energy of the photon emitted in the RDEC process is roughly double that for REC. Thus, the emission of two REC photons detected simultaneously would be nearly indistinguishable from a single RDEC photon. However, the cross section for double REC scales as $(\sigma_{REC}/a_0)^2$ (with $\sigma_{REC} \ll a_0$) [16], making the probability of double REC observation at least two orders of magnitude smaller than that for RDEC.

Photon emission due to REC into the K shell of bare ions was shown to be linearly polarized [17, 18], introducing an angular dependence of $\sin^2 \theta$ between the differential and total cross sections. If the RDEC cross sections behave similarly, the differential cross sections measured here must be multiplied by $8\pi/3$ to get the total cross sections. However, electron correlation in RDEC may affect the polarization of the emitted photon. A detailed study of RDEC polarization would be useful, but very difficult given the small cross sections involved.

The differential and total RDEC cross sections for 2.11 MeV/u F^{9+} and $F^{8+}+N_2$ and Ne are listed in Table II. The RDEC cross sections show large differences with the charge state, with those for F^{8+} being $\sim$6 times smaller than those for F^{9+}. These differences are attributed partially to the number of initial projectile K-shell vacancies and the consequently disallowed RDEC transitions.

Fig. 6 shows the present experimental results for N_2 and Ne gas targets, and the previous experimental and theoretical results for fully-stripped projectiles on thin-foil C targets. The experimental results for the C targets are likely not correct due to the charge state of the exiting RDEC events being increased one or two times (two not measured) due to the high probability of multiple collisions. With this uncertainty, the results for RDEC

TABLE II. RDEC differential ($\frac{d\sigma}{d\Omega}$) (barns/sr) and total (σ) (barns) cross sections for 2.11 MeV/u $F^{9+,8+} + N_2$ and Ne.

	N_2		Ne	
	$\frac{d\sigma}{d\Omega}$	σ	$\frac{d\sigma^*}{d\Omega}$	σ^*
F^{9+}	0.30(17)	2.5(1.4)	0.25(14)	2.1(1.2)
F^{8+}	0.05(3)	0.42(25)	0.04(2)	0.33(20)

*These cross sections may be underestimated by up to a factor of about 2 because the KK $\rightarrow$ KL transition under the REC peak could not be seen.

with F^{9+} on N_2 and Ne are factors of $\sim$2 (for O^{8+}) and 4 (for F^{9+}) times smaller than those reported for the carbon target, although the value for F^{9+} on Ne may be somewhat larger (see Table II). The theories underestimate the experimental data by one to three orders of magnitude. This is likely due to the assumptions made in the theories to simplify the calculations. The work of Ref. [14] employs the line-profile approach for the models shown, both with homogeneous target electron densities: model A considers all the target electrons equally and model K considers only the target K-shell electrons. There are presently no calculations for F^{9+} on gas targets but it is expected that they would not differ greatly from those for carbon.

Investigation of RDEC for the capture of the two K-shell electrons in He targets would be highly desirable, as only two transitions are possible, namely KK$\rightarrow$KK and KK$\rightarrow$KL (only the KK$\rightarrow$KL would be possible for F^{8+} projectiles). As mentioned above, measurements were attempted but stopped because of the very low counting rate, giving just three RDEC events in two weeks.

In summary, RDEC has been observed for 2.11 MeV/u F^{9+} and F^{8+} incident ions on N_2 and Ne gas targets, avoiding multiple-collision effects present in the earlier studies with thin-foil carbon targets. Contaminants are
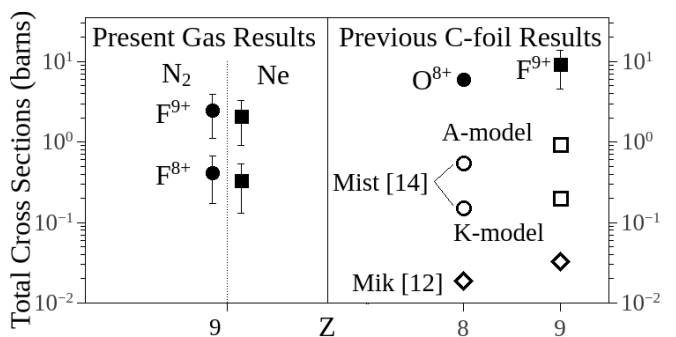

FIG. 6. Present results for N_2 and Ne targets (left panel); previous results for fully-stripped projectiles on thin-foil C targets (right panel). The cross sections obtained for the C targets are uncertain due to multiple collisions (see text). The A- and K-models of the theory are from Ref. [14].

essentially eliminated for gas targets. The presence of one K-shell vacancy instead of two in the incident ion was found to significantly lower (by a factor of ∼6) the RDEC cross sections. Comparison of bare fluorine on gas targets with previous experimental results for O^{8+} and F^{9+} on carbon showed smaller cross sections by factors of about 2-4 for the present results. No theory yet exists specifically for the collision systems done here.

——————

[*] david.s.lamantia@wmich.edu

[1] J. Miraglia and M. S. Gravielle, *International Conference on Photonic, Electronic and Atomic Collisions XV: Book of Abstracts* (1987) p. 517, Brighton, U.K.

[2] A. Simon, A. Warczak, T. Elkafrawy, and J. A. Tanis, Phys. Rev. Lett. **104**, 123001 (2010).

[3] T. Elkafrawy, A. Simon, J. A. Tanis, and A. Warczak, Phys. Rev. A **94**, 042705 (2016).

[4] H. W. Schnopper, H. D. Betz, J. P. Delvaille, K. Kalata, A. R. Sohval, K. W. Jones, and H. E. Wegner, Phys. Rev. Lett. **29**, 898 (1972).

[5] T. Stöhlker *et al.*, Phys. Rev. A **51**, 2098 (1995).

[6] F. Biggs, L. B. Mendelsohn, and J. B. Mann, Atomic Data and Nuclear Data Tables **16**, 201 (1975).

[7] A. Warczak *et al.*, Nuclear Instruments and Methods in Physics Research B **98**, 303 (1995).

[8] G. Bednarz *et al.*, Nuclear Instruments and Methods in Physics Research B **205**, 573 (2003).

[9] N. Winters *et al.*, Physica Scripta **T156** (2013).

[10] V. L. Yakhontov and M. Y. Amusia, Physics Letters A **221**, 328 (1996).

[11] V. L. Yakhontov and M. Y. Amusia, Phys. Rev. A **55**, 1952 (1997).

[12] A. I. Mikhailov, I. A. Mikhailov, A. N. Moskalev, A. V. Nefiodov, G. Plunien, and G. Soff, Phys. Rev. A **69**, 032703 (2004).

[13] A. V. Nefiodov, A. I. Mikhailov, and G. Plunien, Physics Letters A **346**, 158 (2005).

[14] E. A. Mistonova and O. Y. Andreev, Phys. Rev. A **87**, 034702 (2013).

[15] D. S. La Mantia, P. N. S. Kumara, A. Kayani, and J. A. Tanis, X-Ray Spectrometery , 1 (2019), (see Fig. 1).

[16] W. E. Meyerhof, R. Anholt, J. Eichler, H. Gould, C. Munger, J. Alonso, P. Thieberger, and H. E. Wegner, Phys. Rev. A **32**, 3291 (1985).

[17] R. Anholt *et al.*, Phys. Rev. Lett. **53**, 234 (1984).

[18] S. Tashenov *et al.*, Phys. Rev. Lett. **97**, 223202 (2006).